ADVANCED MATERIALS
www.advmat.de

In Situ Multi-Directional Liquid Manipulation Enabled by 3D Asymmetric Fang-Structured Surface

Siqi Sun, Yiyuan Zhang, Shuangmei Wu, and Liqiu Wang**

Decorating surfaces with wetting gradients or topological structures is a prevailing strategy to control uni-directional spreading without energy input. However, current methods, limited by fixed design, cannot achieve multi-directional control of liquids, posing challenges to practical applications. Here, a structured surface composed of arrayed three-dimensional asymmetric fang-structured units is reported that enable in situ control of customized multi-directional spreading for different surface tension liquids, exhibiting five novel modes. This is attributed to bottom-up distributed multi-curvature features of surface units, which create varied Laplace pressure gradients to guide the spreading of different-wettability liquids along specific directions. The surface's capability to respond to liquid properties for multimodal control leads to innovative functions that are absent in conventional structured surfaces. Selective multi-path circuits can be constructed by taking advantage of rich liquid behaviors with the surface; surface tensions of wetting liquids can be portably indicated with a resolution scope of 0.3–3.4 mN m^{-1} using the surface; temperature-mediated change of liquid properties is utilized to smartly manipulate liquid behavior and achieve the spatiotemporal-controllable targeted cooling of the surface at its heated state. These novel applications open new avenues for developing advanced surfaces for liquid manipulation.

1. Introduction

Manipulating liquids to achieve spontaneously directional spreading is prevalent and crucial in numerous practical applications, including fog harvesting,[1] enhanced heat transfer,[2–4] chemical reaction,[5,6] and biomolecular analysis.[7,8] As a widespread occurrence in nature, liquids directionally spread on various organisms' surfaces, including the beak of shorebirds,[9] butterfly wings,[10] spider silk,[11] and cactus spine.[12] Learning from features on these naturally evolved surfaces, numerous theoretical and experimental endeavors have demonstrated the viability of controlling liquids through surfaces with wetting or topographic gradients.[13–17] Specifically, liquid is prone to spread from high side of dynamic-contact-angle to the low side on the anisotropic wetting surface because of the surface energy gradient;[18] from the area with a strong curvature to the one with a weak curvature on the conical structured surface due to Laplace pressure gradient;[19,20] from bottom space to top space on the wedge corner of the microcavity surface resulting from capillary rise effect.[21–23] However, surface-gradient-dominated liquid control limits the spreading direction to a predefined single trajectory.

To date, some efforts have been made to achieve direction-tunable liquid manipulation. For instance, external energies such as light,[24,25] vibration,[26] electricity,[27,28] magnetism,[29–31] and pneumatic actuation,[32] were employed to adjust liquid behaviors flexibly. However, the inherent drawbacks of these strategies lie in their complex control modules and limited validity to materials. Several studies have combined the intrinsic properties of liquids with cross-scale surface structure design to control the multi-directional spreading of different liquids.[33–36] Nevertheless, the driving force for liquid manipulation is still restricted to 1D unbalanced forces acting along two opposite directions, thus limiting the liquid spreading modes to be tunable only within 1D dual directions. As a result, the underexplored liquid behavior limits the functional development in practical scenarios.

In this work, we present a surface composed of arrayed 3D asymmetric fang-structured units (Figures S1–S4, Supporting Information) that successfully manipulate liquids with different surface tensions (22–72 mN m^{-1}) to autonomously select specific spreading directions and exhibit five novel modes (**Figure 1A**; Video S1, Supporting Information). The sophisticated units (Figure 1B-i), integrated on the substrate, are designed with bottom-up 3D multiple curvature features (Figure 1B-ii) with a semicircle bottom and eccentric cone tip (point t), leading to the asymmetry along *xz*-, *yz*-, and *xy*-planes. These curvature features alternately induce Laplace pressure gradients to control the spreading of liquids with different wettability along two

S. Sun, Y. Zhang, S. Wu, L. Wang
Department of Mechanical Engineering
The Hong Kong Polytechnic University
Hong Kong 999077, China
E-mail: yi-yuan.zhang@polyu.edu.hk; liqiu.wang@polyu.edu.hk

The ORCID identification number(s) for the author(s) of this article can be found under https://doi.org/10.1002/adma.202407034

DOI: 10.1002/adma.202407034

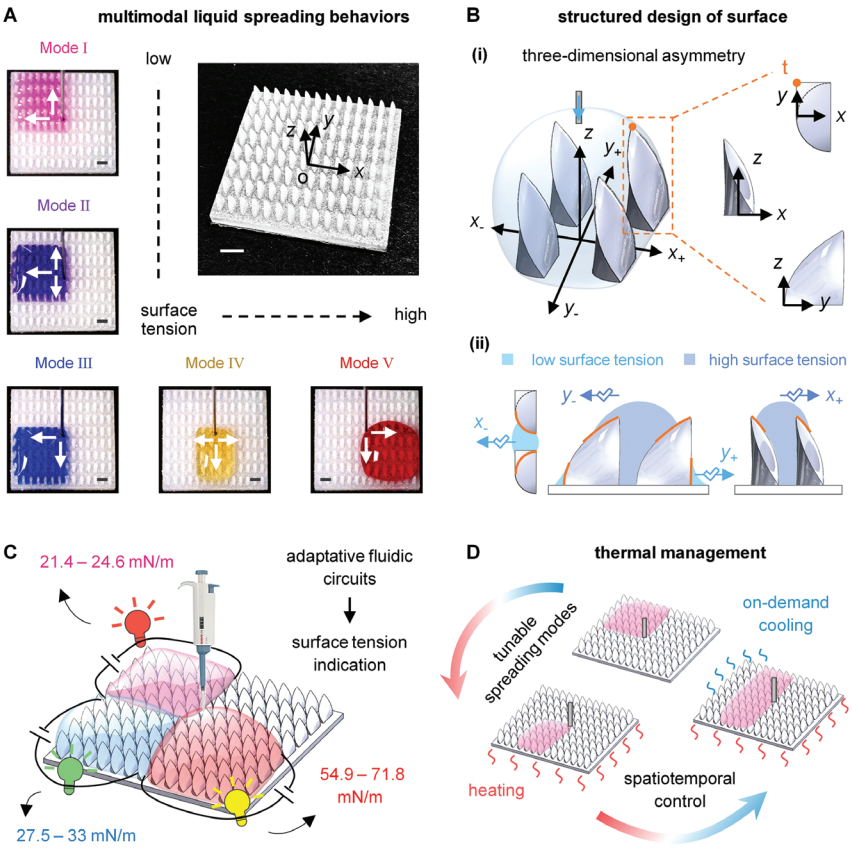

Figure 1. Multimodal liquid spreading behaviors on well-designed fang-structured surface. A) Five spreading modes of liquids with surface tension from 22 to 72 mN m^{-1} and optical image of fang-structured surface. The injection rate is 300 µL min^{-1}. Scale bar, 2 mm. B) Illustration of i) multi-asymmetric structural unit and ii) units' curvature features that dominate the spreading of liquids with different surface tensions in *x* and *y*-directions. C) Schematics of the surface as adaptative fluidic circuits and liquid surface tension indicator. D) Demonstration of surface as a platform for thermal management, including dynamic adjustment of spreading modes and spatiotemporal-controllable targeted cooling.

perpendicular axes (*x*-axis and *y*-axis). In contrast to traditional strategies for multi-directional liquid manipulation that rely on surface structure rearrangement, our surface can simultaneously control multi-directional liquid spreading under a fixed arrangement, i.e., in situ control. This unique capability enables the construction of more complex multi-path circuits adaptive to the conductive liquids' properties. Such adaptability further empowers the surface to achieve portable and precise identification of liquid surface tension range through carefully designed geometrical parameters (Figure 1C). Under high-temperature conditions (such as 140 °C), this surface enhances liquid manipulation to dynamically regulate the spreading directions by effectively utilizing evaporation-mediated change in the liquid property, thus achieving spatiotemporally controlled targeted cooling of the heated platform (Figure 1D). This work, for the first time, achieves in situ control of multi-directional liquid spreading, opening avenues for advanced liquid manipulation surfaces.

2. Results and Discussion

2.1. Mechanism of Multimodal Spreading

To comprehend the multimodal spreading of liquids, we investigate the mechanism underlying liquids' proceeding behaviors along different directions. Once liquid is injected on the surface, it fills the space formed by four adjacent units, forming unequal curvature of the liquid meniscus with units' curvature structure, leading to differences in Laplace pressure at various positions on the liquid surface. Such Laplace pressure gradients determine liquids' preferential spreading directions. With surface tension from low to high, liquids exhibit spreading with Mode I to Mode V respectively. Here, by describing the liquid forefront proceeding in *x* and *y*-directions, we first investigate the three single-quadrant spreading types (Modes I, III, and V) and subsequently elucidate the two cross-quadrant spreading types (Modes II and IV).

In Mode I, the injected liquid with low surface tension spreads along the second quadrant on the fang-structured surface. The high wettability facilitates the adhesion of liquid to the fang-structured units and interacts with the bottom semicircle curvature of units (Video S1, Supporting Information). In *x*-direction, liquid forms convex meniscus with different curvature in x_- and x_+ directions (**Figure 2A-i**), yielding opposite and unequal Laplace pressures Δp_{1x-} and Δp_{1x+}:

$$\Delta p_{1x-} = \frac{\gamma_1}{r_{1x-}} < \Delta p_{1x+} = \frac{\gamma_1}{r_{1x+}} \quad (1)$$

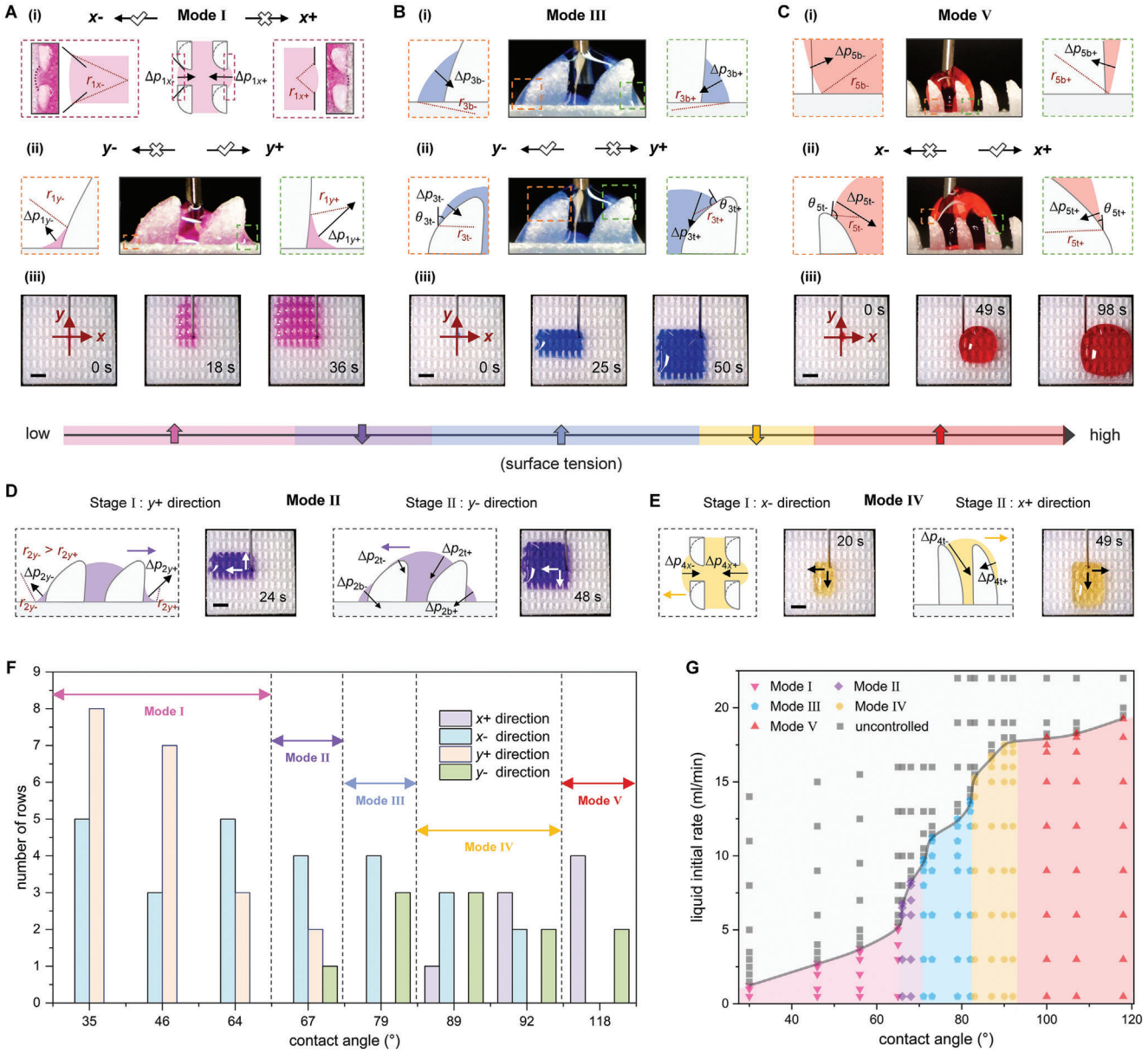

Figure 2. Mechanisms underlying the multi-modal spreading behaviors on the surface. Investigation of Laplace pressure gradients of five liquid spreading modes formed by specific units' curvature features and liquid, along *x* and *y*-directions. The injection rate is 300 µL min^{-1}. A) Mode I. The units' semicircular structure in the *xy*-plane and bottom curvature structure in *yz*-plane rectify the liquid in i) *x* the ii) *y*-directions, respectively; iii) Spreading phenomenon of 90% ethanol and 10% DI water. Scale bar, 3.5 mm. B) Mode III. The curvature structure of the unit's i) bottom and ii) cone tip in the *yz*-plane dominate rectification along the *y*-direction. iii) Spreading behavior of 40% ethanol-60% DI water mixture. Scale bar, 3.5 mm. C) Mode V. The unit's i) bottom and ii) tip curvature in the *xz*-plane causes liquid reentrant in the x_+ direction, and iii) the corresponding experimental phenomenon with DI water. Scale bar, 3.5 mm. D), E) Mode II and Mode IV. Mechanisms analysis and spreading behaviors of 55% ethanol-45% DI water mixture and 25% ethanol-75% DI water mixture respectively. Scale bar, 3.5 mm. F) Illustration of the spreading shape variation of different-contact-angle liquids by exhibiting their spreading number of rows in negative and positive x- and y-directions. G) Illustration of the effect of initial injection flow rate on five spreading modes.

where γ_1 is liquid surface tension, r_{1x-} and r_{1x+} are the local curvature radii of liquid forefront. The contrast of these two Laplace pressures depends on r_{1x-} and r_{1x+} ($r_{1x-} > r_{1x+}$) and the comparison is illustrated in Figure S5 (Supporting Information). The unbalanced Laplace pressures give rise to the smaller resistance in the negative *x*-direction; as injection proceeds, liquid continuously spreads in this direction, reaching the next row of units, then repeating this process (Figure S5, Supporting Information). Along the *y*-direction, Figure 2A-ii, the units' bottom curvature structure in the *yz*-plane causes the liquid to form concave meniscus with different local curvature (Video S2, Supporting Information), resulting in two opposite and unequal Laplace pressures in

y_- (Δp_{1y-}) and y_+ (Δp_{1y+}) directions (Figure S6, Supporting Information):

$$\Delta p_{1y-} = \frac{\gamma_1}{r_{1y-}} < \Delta p_{1y+} = \frac{\gamma_1}{r_{1y+}} \quad (2)$$

where r_{1y-} and r_{1y+} are the local curvature radii of the liquid surface. The larger Laplace pressure in the y_+ direction is the driving force, determining the continuously directional spreading (Video S2, Supporting Information). This mode is illustrated in Figure 2A-iii with a mixture of 90% ethanol and 10% deionized (DI) water as the test liquid, spreading in the second quadrant. Additionally, liquid surface tension remains stable during the experiment (Figure S7, Supporting Information).

The liquid spreading with Mode III is along the third quadrant on a fang-structured surface. The bottom semicircle structure of fang-structured units still determines the spreading along the x-direction, thus liquid in Mode III forms the convex meniscus with similar local curvature with Mode I, leading to a similar Laplace pressure gradient (Figure S8 and Video S2, Supporting Information). Therefore, liquid preferentially spreads in the negative x-direction. For proceeding along the y-direction, the liquid surrounding the bottom of units forms a convex meniscus and generates the opposite and equal Laplace pressures Δp_{3b-} and Δp_{3b+} which pin the spreading along units' bottom (Figure 2B-i). Therefore, the continuously injected liquid accumulates above the units' top, resulting in the curvature structure of the unit's cone tip in the yz-plane dominating rectification along the y-direction (Video S1, Supporting Information). Consequently, liquid forms unequal dynamic contact angles ($\theta_{3t-} < \theta_{3t+}$) (Figure 2B-ii). The smaller dynamic contact angle means the smaller local curvature ($r_{3t-} > r_{3t+}$) which induces the lower Laplace pressure ($\Delta p_{3t-} < \Delta p_{3t+}$), thus liquid continuously reentrant into the surface in the y_- direction (Video S2, Supporting Information). As shown in Figure 2B-iii, a mixture of 40% ethanol and 60% DI water spread in the third quadrant on the surface.

The liquid with a higher surface tension spreads with Mode V, along the fourth quadrant on the fang-structured surface. The lower wettability hinders the spreading of liquids along the units' bottom structures, thus weakening their rectification and leading to the curvature structures of cone tip in xz-and yz-planes that dominate the spreading along the x and y-directions, respectively (Video S1, Supporting Information). In y-direction, liquid forms the convex meniscus with a similar curvature gradient with Mode III, thus directionally spread in the negative y-direction (Figure S8, Supporting Information). Along the x-direction, after forming convex meniscus surrounding the bottom of units, the opposite Laplace pressures ($\Delta p_{5b-} = \Delta p_{5b+}$) resist liquid spreading (Figure 2C-i), thus liquid accumulates and interacts with the curvature structures of units' cone tip. The unequal local curvature ($\theta_{5t-} > \theta_{5t+}$, $r_{5t-} < r_{5t+}$) of the formed liquid meniscus determines smaller Laplace pressure in the positive x-direction ($\Delta p_{5t-} > \Delta p_{5t+}$) (Figure 2C-ii), leading to liquid directional spreading (Video S2, Supporting Information). Figure 2C-iii shows the continuous flow in the fourth quadrant with DI water as the test liquid.

The liquid with its surface tension between those in Mode I and Mode III spreads with Mode II, such as a mixture of 55% ethanol and 45% DI water, displays two spreading stages along the second and third quadrant sequentially. The main transition occurs in the y-direction. (Figure 2D). In Stage I, it spreads along the y_+ direction driven by the larger Laplace pressure ($\Delta p_{2y-} < \Delta p_{2y+}$) during the first 24 s. It then transfers into Stage II until 48 s; as the continuously injected liquid forms a convex surface, the Laplace pressures at the bottom ($\Delta p_{2b-} = \Delta p_{2b+}$) begin to pin the liquid, then liquid reentrant in the y_- direction where Laplace pressure ($\Delta p_{2t-} < \Delta p_{2t+}$) is lower, caused by smaller local liquid meniscus curvature.

Another cross-quadrant spreading type, Mode IV, occurs with liquids of surface tension between those in Mode III and Mode V. Its spreading behavior is first along the third quadrant and then along the fourth quadrant, and the main change happens in the x-direction. Examined by the mixture of 25% ethanol and 75% DI water (Figure 2E), in the first 20 s (Stage I), the liquid proceeds in the negative x-direction due to the Laplace pressure gradient ($\Delta p_{4x-} < \Delta p_{4x+}$) which transfers to equal resistant forces as the liquid accumulation. It then changes to Stage II until 49 s, smaller Laplace pressure ($\Delta p_{4t+} < \Delta p_{4t-}$) causes liquid reentrant along the x_+ direction.

To sum up, the liquid surface tension (i.e., the wettability) determines the dominating curvature structures among the multiple curvature features of fang-structured units, yielding the five spreading modes (Figure 1B-ii; Video S1, Supporting Information). Moreover, during the liquid spreading process, unbalanced adhesion forces may induce minor elastic deformation of the fang-structured units along the x-direction. However, this effect is negligible and does not occur at the critical moment that enables the directional spreading. Therefore, the minor structure deformation has a negligible effect on the liquid spreading behaviors (see details in Figures S9 and S10 and Video S2, Supporting Information).

We further illustrate the spreading shape variation of different-contact-angle liquids by exhibiting their spreading number of rows in negative and positive x- and y-directions (Figure 2F). A series of equal-volume (150 µL) ethanol–DI water binary mixtures are injected, with contact angles from 35° to 118°, they spread along the second to fourth quadrants on the surface, following Mode I to Mode V, respectively. As the contact angle increases, the decreased spreading areas demonstrate liquid accumulation to higher heights, exhibiting reentrant spreading behaviors and slower spreading velocities (Figure S11, Supporting Information). As various injection flow rates may be involved in applications, we evaluate the critical liquid injection flow rates necessary to maintain these five spreading modes (Figure 2G). Once beyond the critical injection flow rates, the inertial force will become unignorable and give rise to the liquid motion without preferential directions.

2.2. Adaptive Liquid Circuits

The surface's ability to control different spreading trajectories for specific surface tension liquids enables the construction of multi-path fluidic circuits using only one piece of surface instead of assembling multiple liquid control modules.[37,38] As shown in **Figure 3A**, the conductive liquids (ethanol-DI water binary liquid with 0.5 g L^{-1} potassium hydroxide) spread along distinct quadrants on the surface, selectively switch on the isolated

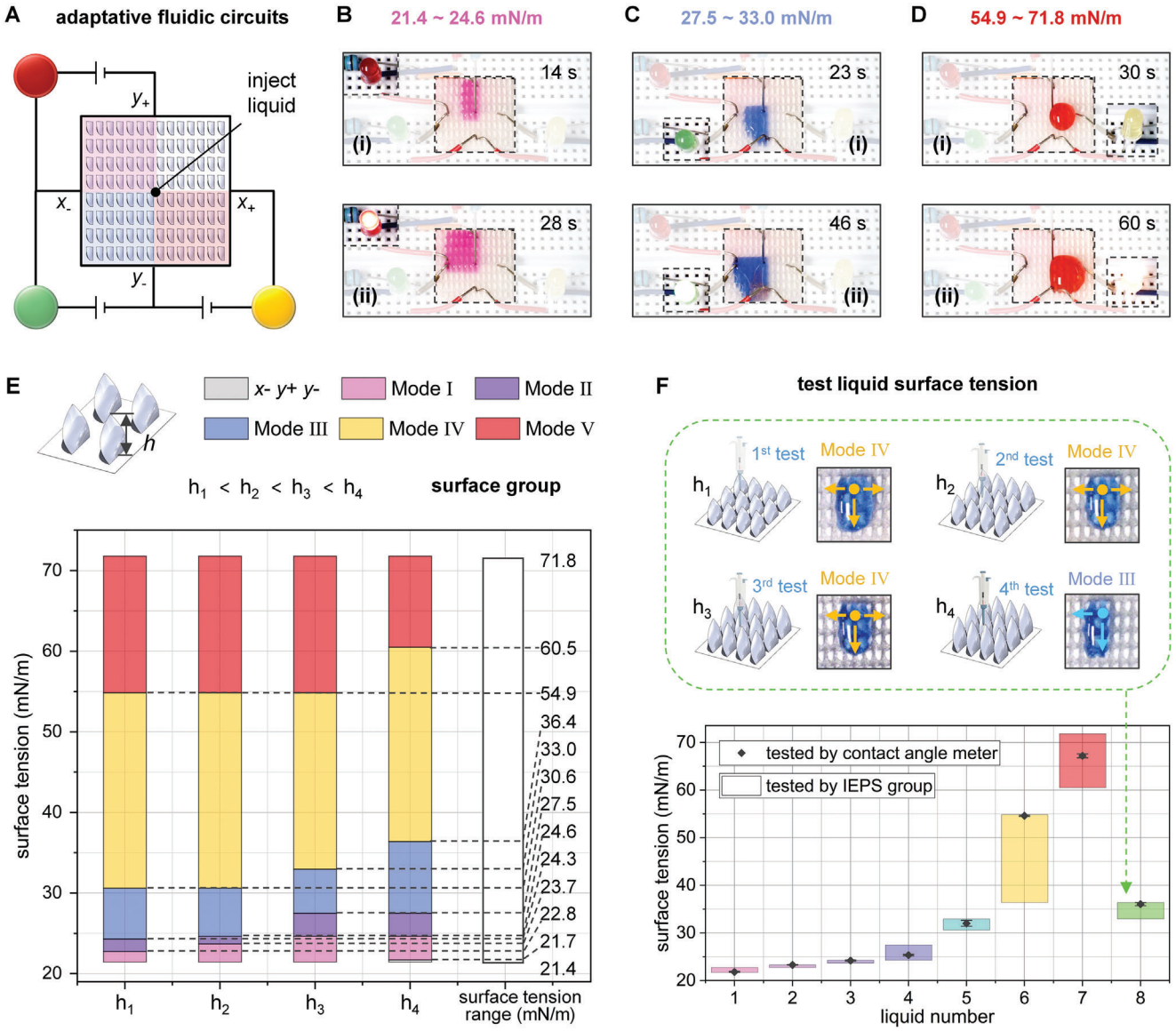

Figure 3. Adaptive liquid circuits and portable surface tension indication based on the smart response ability of the surface. A) Illustration of the complex fluidic circuits constructed by the conductive liquids with specific surface tensions. B–D) Experimental phenomenon of selectively connecting the isolated circuit and lighting the corresponding LED bulb. The injection rate is 300 μL min^{-1}. E) Portable surface tension indication by the surface group consisting of four pieces of surface with different unit heights, and the created surface tension database. F) Demonstration of surface tension testing procedure utilizing surface group and testing results of eight kinds of liquid.

circuit and light up the relative LED bulbs (Video S3, Supporting Information). A mixture of 90% ethanol and 10% DI water (21.7 mN m^{-1}) reaches the y_+ electrode in 14s (Figure 3B-i), connecting to the x_- electrode and lighting up the red bulb in 28s (Figure 3B-ii). Similarly, liquids with surface tension between 21.4 mN m^{-1} and 24.6 mN m^{-1} spread along the second quadrant and light up the red bulb. A mixture of 40% ethanol and 60% DI water (27.5 mN m^{-1}) takes 23 s to reach the y_- electrode (Figure 3C-i) and then connects to the x_- electrode, resulting in the illumination of the green bulb after 46 s (Figure 3C-ii). Liquids with surface tension range from 27.5 to 33.0 mN m^{-1} spread along the third quadrant and also light up the green bulb. DI water (71.8 mN m^{-1}) requires 30 s to reach the x_+ electrode (Figure 3D-i), followed by a connection to the y_- electrode and lights up the yellow bulb in 60 s (Figure 3D-ii). Liquids with surface tension between 54.9 and 71.8 mN m^{-1} spread along the fourth quadrant and light up this yellow bulb. Such characteristic of adaptive liquid surface tension removes the difficulty of complex circuit construction, showing the capability of this surface response to liquids with different surface tensions.

2.3. Portable Surface Tension Indicator

Building upon the surface's capability response to liquid property and control over the specific spreading mode, we further develop

a group of surfaces with different units' heights ($h_1 < h_2 < h_3 < h_4$) for portable surface tension indication without involving any expensive quantitative and detecting instruments. These surfaces allow liquids to perform distinct spreading modes, but the units' height difference results in slight variations in the critical surface tensions for mode transition (Figures S12–S14, Supporting Information). As a result, the mode-based classification of surface tension ranges can be refined by combining the spreading modes on these surfaces, thereby improving the indication accuracy. We use a series of ethanol-DI water binary mixtures to calibrate the surface tension ranges for five modes on the surface group and create the surface tension database (Figure 3E), consisting of twelve ranges covering 21.4–71.8 mN m^{-1}. This database demonstrates excellent indication capability for low surface tension ranges, with an accuracy of 0.3–3.4 mN m^{-1} for surface tension values ranging from 21.4 to 36.4 mN m^{-1}. Such specific accuracy can be explained by the nonlinear relationship between surface tension and contact angle (Figure S13, Supporting Information) which indicates that only a smaller surface tension value is needed to reach the contact angle that changes the spreading to reentrant mode (Figure S12, Supporting Information).

To verify the validation as the surface tension indicator, we use the surface group to test eight kinds of liquids (Figure S15, Supporting Information), as shown in Figure 3F. The test was performed by a pipette gun, absorbing 160 µL of the test liquid which is the minimum volume that meets the identification of spreading mode (Figure S16, Supporting Information), and slowly injecting on the surface group. The results of the surface tension range can be obtained by referring to the database. Take the eighth liquid as an example (Video S3, Supporting Information), it spreads with Mode IV on the surface with the unit's height of h_1, h_2, and h_3, and Mode III on the h_4-height surface, so the surface tension falls in 33.0–36.4 mN m^{-1}. The results of these liquids tested by our surface group are in good agreement with those tested by the surface tension meter (Figure S17, Supporting Information). This surface group, as a surface tension indicator, illustrates the instrumental functionality that senses the properties of unknown liquids only through their spreading behaviors. Such sensing capability is often overlooked in traditional liquid rectifiers, providing a new idea for functionalizing liquid manipulation surfaces.

2.4. On-Demand Thermal Management Through Dynamic Liquid Regulation

Temperature control serves as one of the foundations for manipulating liquid behavior and is crucial for various manufacturing processes and intelligent applications.[39–43] However, in the domain of controlling liquid directional spreading with structured surfaces, an often-overlooked yet critical phenomenon is the temperature-induced changes in liquid properties.[14] For instance, in the classic phenomenon known as the "tears of wine",[44] the evaporation of ethanol in an ethanol–water mixture results in a significant alteration of surface tension. This inherent characteristic change in liquids, inevitable in practical heat exchange applications, poses challenges to the directional liquid manipulation of conventional surfaces. Here, our surface can maintain effective control of liquid spreading, and even utilize the surface tension change to dynamically control liquid spreading directions with one piece of static surface, thus achieving spatiotemporal controllable targeted cooling on demand.

The experimental setup for investigating thermal controlled spreading behaviors and their cooling effects is depicted in Figure S18 (Supporting Information). When the mixture of 53% ethanol and 47% DI water (Liquid I) is injected on a surface undergoing heating from 25 to 94 °C in temperature (injection rate: 50 µL min^{-1}), it performs three-stage spreading behavior (**Figure 4A**; Video S4, Supporting Information). During Stage I, Liquid I spreads along the negative *x*-direction, and then along the second quadrant in Stage II, finally transfers to spread along the third quadrant in Stage III. The spreading shift also occurs for 30% ethanol-70% DI water mixture (Liquid II) at an injection rate of 50 µL min^{-1} during heating of the surface to a higher temperature (from 80 to 120 °C), which consists of four stages (Figure 4B; Video S4, Supporting Information): In Stage I, Liquid II spreads along the negative *x*-direction, and then along the negative *y*-direction within quadrant III in Stage II; In Stage III, it begins to spread along positive *x*-direction within the quadrant IV; In Stage IV, it spreads along the negative *y*-direction within both Quadrant III and IV.

The primary cause for these dynamic spreading behaviors can be attributed to evaporation-induced changes in the liquid surface tension (Figure 4C; Video S4, Supporting Information). For the ethanol-DI water mixture that is injected onto the fang-structured surface, ethanol evaporates more easily than water during the heating process, causing an increase in the proportion of water and thus a larger surface tension (Figure S19, Supporting Information). As the ethanol-DI water mixture is continuously injected into the liquid on a fang-structured surface, the surface tension gradient is formed between the newly injected liquid (with lower surface tension) and the original liquid (with higher surface tension). Due to the Marangoni effect, the newly injected ethanol-DI water mixture spreads toward the original liquid, resulting in an increase in the overall surface tension of the liquid on the fang-structured surface and transferring the spreading behavior. We select the maximum surface tension liquid (Liquid I) that spreads along Quadrant II (Mode I) at room temperature to demonstrate this dynamic spreading behavior. Since the surface tension range covered by liquids in Mode II is only 2.9 mN m^{-1}, when Liquid I is injected on a surface at a temperature of 90 °C, its surface tension can be increased beyond this value, leading to a transition of spreading behavior directly from Mode I to Mode III (from quadrant II to III). For liquids spreading in the third quadrant (Mode III) at room temperature, the large surface tension range associated with Mode IV (21.9 mN m^{-1}) hinders them from performing cross-mode spreading transition, and liquids require a higher temperature (such as 120 °C) to exhibit dynamic spreading behavior. As exhibited by Liquid II, it spreads in the third quadrant and then switches to the fourth quadrant on a surface at a temperature of 120 °C. Compared to spreading on a surface undergoing heating from 80 to 120 °C in temperature, the transition of the spreading quadrant occurs 10 s earlier (Figure S20, Supporting Information).

We further investigate the temperature conditions under which the spreading behaviors of the above two liquids change, where the initial injection flow rate is a crucial factor that requires

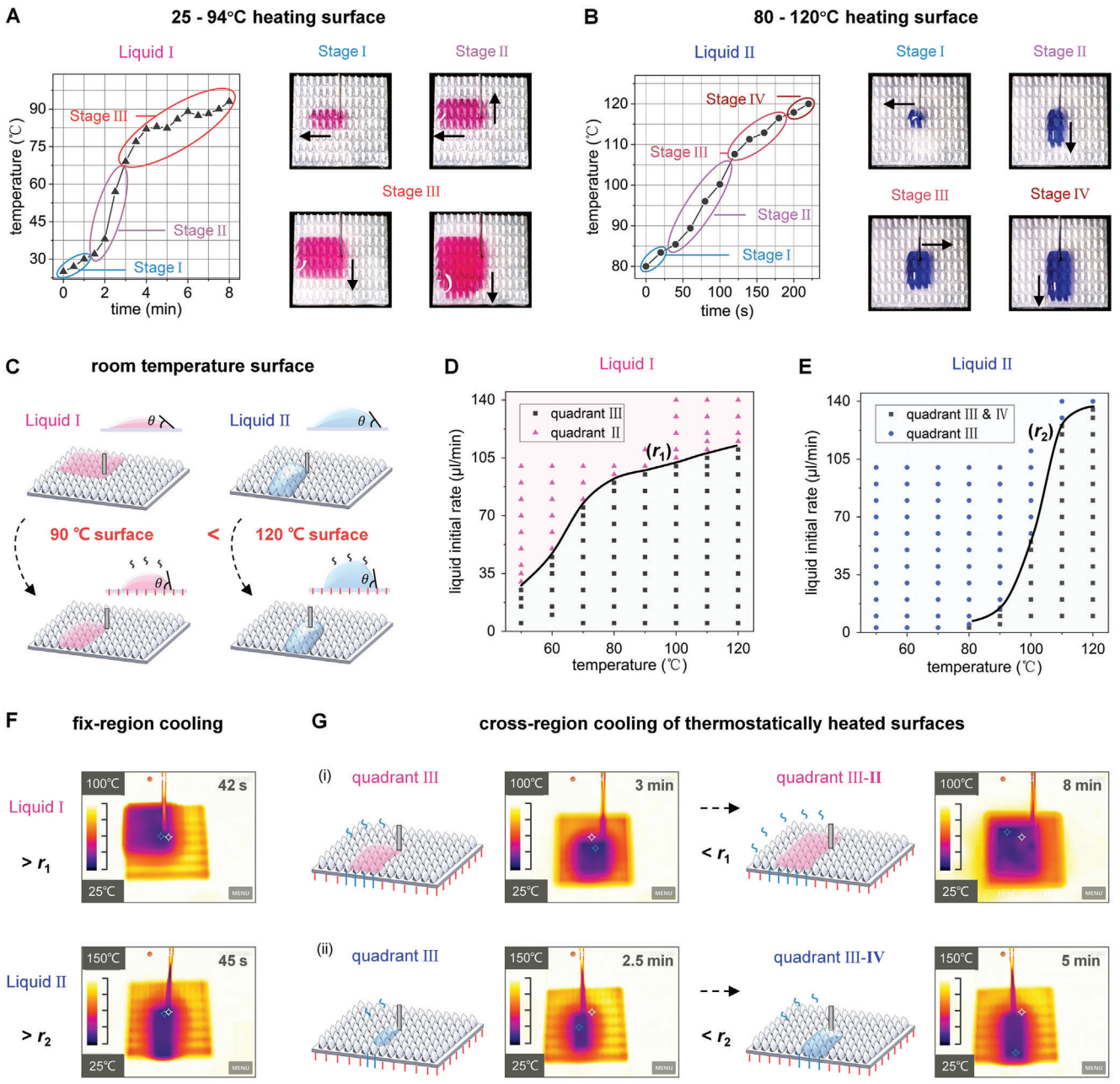

Figure 4. Dynamic liquid regulation and on-demand thermal management. A) Dynamic spreading behavior of Liquid I during the heating process (on the surface heated from 25 to 94 °C in temperature). B) The spreading behavior of Liquid II on the surface heated from 80 to 120 °C in temperature. C) Mechanisms of spreading behaviors transfer. D), E) Demonstration of the initial injection flow rates on different heating-temperature surfaces that cause the spreading behaviors transition of Liquid I and II. (F) The fix-region cooling of the surface: injecting Liquid I on the surface at a temperature of 90 °C, and injecting Liquid II into the surface at a temperature of 110 °C. (G) The cross-region cooling of the surface by slowly injecting Liquid I (95 μL min^{-1}) and Liquid II (50 μL min^{-1}) on the surface at a temperature of 90 and 110 °C, respectively.

careful consideration. As shown in Figure 4D,E, we heat the surface to a series of constant temperatures and inject Liquid I and II at a range of initial injection flow rates, then identify the threshold (r_1 for Liquid I, r_2 for Liquid II) smaller than which the spreading behavior undergoes a transition. On the lower-temperature surface, the surface temperature is not sufficient to cause a rapid reduction in ethanol content, necessitating a slower injection rate to increase the duration of heat exchange between the liquid and the heating substrate, thereby increasing liquid surface tension sufficiently to transfer the spreading quadrant. Especially for Liquid II, on the surface with temperatures below 80 °C, it cannot change its spreading behavior even at extremely slow injection flow rates (<1 μL min^{-1}), and requires a smaller injection rate than Liquid I on 80–100 °C surface. By contrast, Liquid II can shift its spreading behavior with a larger injection rate on a surface undergoing heating from 110 to 120 °C in temperature. This

is because Liquid I need to transfer spreading from quadrant II to quadrant III once injected on the surface, and the time for thermal exchange is much shorter than Liquid II that slowly transfers from Quadrant III to Quadrant IV. Considering the diverse liquids and intricate operating conditions that may arise in practical applications, the variability in their spreading behavior depends on whether the changes in their surface tension exceed the defined ranges of the respective spreading modes (Figure S21, Supporting Information).

Given the surface's ability to dynamically control liquids for tunable multimodal spreading behaviors, it can be utilized to achieve liquid-based spatiotemporally controllable cooling of thermostatically heated surfaces, including selectable fixed-region cooling and cross-region sequential cooling. For example, as the initial injection rate is larger than r_1 (e.g., 200 µL min^{-1}), Liquid I remains spreading along the second quadrant on the surface at a temperature of 90 °C and cooling the liquid-covered region (Figure 4F); Quadrant III of the surface at a temperature of 110 °C can be cooled by Liquid II with an initial injection rate greater than r_2 (e.g., 200 µL min^{-1}) (Figure 4F). When reducing the injection rate to a value below the threshold, Liquid I and II will perform cross-region sequential cooling based on dynamic spreading behaviors. As shown in Figure 4G-i (Video S4, Supporting Information), Liquid I first cools the third quadrant of the surface at a temperature of 90 °C, then as surface temperature decreases, begins to cool the second quadrant due to a slower rate of ethanol evaporation. As for Liquid II (Figure 4G-ii; Video S4, Supporting Information), it sequentially cools some parts of the third and fourth quadrants of the surface at a temperature of 110 °C. However, nonvolatile liquids are unable to achieve sequential cooling across different regions due to the limitation that their surface tension cannot be significantly altered by temperature, such as the surface's cooling by DI water in Quadrant IV (Figure S22 and Video S4, Supporting Information). Also, unlike the common cooling situation such as under room temperature (Figure S22 and Video S4, Supporting Information), the injecting liquid enables faster cooling of targeted specific regions (Figure 4F and Video S4, Supporting Information). Therefore, by utilizing liquids with carefully designed surface tension, the fang-structured surface allows for targeted cooling of specific areas on demand.

3. Conclusion

The designed fang-structured units enable liquids with different surface tensions to autonomously select specific spreading quadrants on a fixed arrangement surface. The proposed unit's bottom-up multi-curvature features, customized for liquids' surface tensions, generate Laplace pressure gradients along two perpendicular axes, thereby in situ controlling multi-directional liquids spreading with five novel modes. This control capability enables the easy construction of complex fluidic circuits and endows liquid manipulation surface with instrumental functionality such as the reliable and portable indication of liquid surface tension. Moreover, the surface's effectiveness in controlling liquids' directional spreading under high-temperature conditions positions it as a competitive candidate for practical applications in thermal management. Through changes in liquid properties mediated by evaporation, only one piece of surface can dynamically adjust the liquid spreading directions, thereby achieving spatiotemporal-controllable targeted cooling of the heated platform. The proposed unique controlling strategy can serve as a guideline for designing advanced surfaces for manipulating various liquids. Moreover, it provides new insights into the development of low-energy-consuming intelligent devices such as sensing unknown liquid properties and on-demand thermal management via distinct liquid spreading behaviors.

Supporting Information

Supporting Information is available from the Wiley Online Library or from the author.

Acknowledgements

The authors thank Mr. Kin Wa Lui from the University Research Facility in 3D Printing (U3DP) at The Hong Kong Polytechnic University for his help in printing the molds. The authors would also like to thank the Industrial Centre (IC) at The Hong Kong Polytechnic University for the assistance in measuring contact angle and surface tension. Furthermore, the authors acknowledge the generous financial support provided by the Research Grants Council of Hong Kong (GRF 17213823, 17205421, and 17204420).

Conflict of Interest

The authors declare no conflict of interest.

Data Availability Statement

The data that support the findings of this study are available in the supplementary material of this article.

Keywords

asymmetric fang-structured surface, liquid spreading control, multi-directional liquid manipulation, surface tension

Received: May 17, 2024
Revised: July 1, 2024
Published online: July 26, 2024

[1] Y. Tian, P. Zhu, X. Tang, C. Zhou, J. Wang, T. Kong, M. Xu, L. Wang, *Nat. Commun.* **2017**, *8*, 1080.
[2] W. Li, S. Yang, Y. Chen, C. Li, Z. Wang, *Nat. Commun.* **2023**, *14*, 3996.
[3] W. Li, Z. Wang, F. Yang, T. Alam, M. Jiang, X. Qu, F. Kong, A. S. Khan, M. Liu, M. Alwazzan, Y. Tong, C. Li, *Adv. Mater.* **2020**, *32*, 1905117.
[4] R. V. Erp, R. Soleimanzadeh, L. Nela, G. Kampitsis, E. Matioli, *Nature* **2020**, *585*, 211.
[5] W. Li, X. Tang, L. Wang, *Sci. Adv.* **2020**, *6*, eabc1693.
[6] Y. Zhang, Z. Huang, Z. Cai, Y. Ye, Z. Li, F. Qin, J. Xiao, D. Zhang, Q. Guo, Y. Song, J. Yang, *Sci. Adv.* **2021**, *7*, eabi7498.
[7] S. Jiang, B. Li, J. Zhao, D. Wu, Y. Zhang, Z. Zhao, Y. Zhang, H. Yu, K. Shao, C. Zhang, R. Li, C. Chen, Z. Shen, J. Hu, B. Dong, L. Zhu, J. Li, L. Wang, J. Chu, Y. Hu, *Nat. Commun.* **2023**, *14*, 5455.
[8] Z. Peng, Y. Chen, T. Wu, *ACS Appl. Mater. Interfaces* **2020**, *12*, 47299.

[9] M. Prakash, D. Quere, J. Bush, *Science* **2008**, *320*, 931.
[10] C. Liu, J. Ju, Y. Zheng, L. Jiang, *ACS Nano* **2014**, *8*, 1321.
[11] Y. Zheng, H. Bai, Z. Huang, X. Tian, F. Q. Nie, Y. Zhao, J. Zhai, L. Jiang, *Nature* **2010**, *463*, 640.
[12] J. Ju, H. Bai, Y. Zheng, T. Zhao, R. Fang, L. Jiang, *Nat. Commun.* **2012**, *3*, 1247.
[13] M. Chaudhury, G. M. Whitesides, *Science* **1992**, *256*, 1539.
[14] S. Daniel, M. K. Chaudhury, J. C. Chen, *Science* **2001**, *291*, 633.
[15] X. Tang, W. Li, L. Wang, *Nat. Nanotechnol* **2021**, *16*, 1106.
[16] K. Chu, R. Xiao, E. N. Wang, *Nat. Mater.* **2010**, *9*, 413.
[17] H. Bai, X. Wang, Z. Li, H. Wen, Y. Yang, M. Li, M. Cao, *Adv. Mater.* **2023**, *35*, 2211596.
[18] M. Soltani, K. Golovin, *Adv. Funct. Mater.* **2022**, *32*, 2107465.
[19] E. Lorenceau, D. Quere, *J. Fluid Mech.* **2004**, *510*, 29.
[20] C. Li, C. Yu, S. Zhou, Z. Dong, L. Jiang, *Proc. Natl Acad. Sci. USA* **2020**, *117*, 23436.
[21] H. Chen, P. Zhang, L. Zhang, H. Liu, Y. Jiang, D. Zhang, Z. Han, L. Jiang, *Nature* **2016**, *532*, 85.
[22] H. Chen, T. Ran, Y. Gan, J. Zhou, Y. Zhang, L. Zhang, D. Zhang, L. Jiang, *Nat. Mater.* **2018**, *17*, 935.
[23] L. Wu, L. Wu, Z. Dong, Z. Cai, T. Ganapathy, N. X. Fang, C. Li, C. Yu, Y. Zhang, Y. Song, *Nat. Commun.* **2020**, *11*, 521.
[24] J. Lv, Y. Liu, J. Wei, E. Chen, L. Qin, Y. Yu, *Nature* **2016**, *537*, 179.
[25] K. Ichimura, S.-K. Oh, M. Nakagawa, *Science* **2000**, *288*, 1624.
[26] Z. Yuan, C. Lu, C. Liu, X. Bai, L. Zhao, S. Feng, Y. Liu, *Sci. Adv.* **2023**, *9*, eadg235.
[27] Y. Jin, W. Xu, H. Zhang, R. Li, J. Sun, S. Yang, M. Liu, H. Mao, Z. Wang, *Proc. Natl. Acad. Sci. USA* **2022**, *119*, 2105459119.
[28] S. Zhang, M. Elsayed, R. Peng, Y. Chen, Y. Zhang, J. Peng, W. Li, M. D. Chamberlain, A. Nikitina, S. Yu, X. Liu, S. L. Neale, A. R. Wheeler, *Nat. Commun.* **2021**, *12*, 5349.
[29] A. Li, H. Li, Z. Li, Z. Zhao, K. Li, M. Li, Y. Song, *Sci. Adv.* **2020**, *6*, eaay5808.
[30] J. Zhang, X. Wang, Z. Wang, S. Pan, B. Yi, L. Ai, J. Gao, F. Mugele, X. Yao, *Nat. Commun.* **2021**, *12*, 7136.
[31] J. Miao, *Sens. Actuator A Phys.* **2024**, *368*, 115104.
[32] Y. Si, T. Wang, C. Li, C. Yu, N. Li, C. Gao, Z. Dong, L. Jiang, *ACS Nano* **2018**, *12*, 9214.
[33] J. Miao, T. Zhang, G. Li, D. Guo, S. Sun, R. Tan, J. Shi, Y. Shen, *Engineering* **2023**, *23*, 170.
[34] S. Feng, P. Zhu, H. Zheng, H. Zhan, C. Chen, J. Li, L. Wang, X. Yao, Y. Liu, Z. Wang, *Science* **2021**, *373*, 1344.
[35] J. Sun, X. Qin, Y. Song, Z. Xu, C. Zhang, W. Wang, Z. Wang, B. Wang, Z. Wang, *Int. J. Extrem. Manuf.* **2023**, *5*, 025504.
[36] S. Sun, J. Miao, R. Tan, T. Zhang, G. Li, Y. Shen, *Adv. Funct. Mater.* **2023**, *33*, 2209769.
[37] B. Zhang, J. Li, J. Zhou, L. Chow, G. Zhao, Y. Huang, Z. Ma, Q. Zhang, Y. Yang, C. K. Yiu, J. Li, F. Chun, X. Huang, Y. Gao, P. Wu, S. Jia, H. Li, D. Li, Y. Liu, K. Yao, R. Shi, Z. Chen, B. L. Khoo, W. Yang, F. Wang, Z. Zheng, Z. Wang, X. Yu, *Nature* **2024**, *628*, 84.
[38] J. Hubbard, J. D. Hubbard, R. Acevedo, K. M. Edwards, A. T. Alsharhan, Z. Wen, J. Landry, K. Wang, S. Schaffer, R. D. Sochol, *Sci. Adv.* **2021**, *7*, eabe5257.
[39] N. Cira, A. Benusiglio, M. Prakash, *Nature* **2015**, *519*, 446.
[40] C. Li, C. Yu, D. Hao, L. Wu, Z. Dong, L. Jiang, *Adv. Funct. Mater.* **2018**, *28*, 1707490.
[41] Q. Zhang, Y. Lv, Y. Wang, S. Yu, C. Li, R. Ma, Y. Chen, *Nat. Commun.* **2022**, *13*, 4874.
[42] Y. Jing, Z. Zhao, X. Cao, Q. Sun, Y. Yuan, T. Li, *Nat. Commun.* **2023**, *14*, 8060.
[43] Y. Cui, Z. Qin, H. Wu, M. Li, Y. Hu, *Nat. Commun.* **2021**, *12*, 1284.
[44] J. Thomson, *Philos. Mag.* **1855**, *10*, 330.